Guiding cancer therapy: Rajendran and Mankoff comment on the promise of noninvasive molecular imaging methods, including a tumor hypoxia approach featured in this month's *JNM*, for characterizing biologic processes within individual patients and thereby enhancing clinical decision making. . . . . ***Page 855***

Automating Parkinson's analysis: Zubal and colleagues describe a fully automated striatal analysis program applied to dopamine transporter images in patients with early symptoms of suspected parkinsonism and compare its performance with that of a trained image-processing technologist. . . . . ***Page 857***

^{123}I-SAP retention in amyloidosis: Hazenberg and colleagues assess the diagnostic performance and prognostic value of a simple parameter describing extravascular ^{123}I-SAP retention in systemic amyloidosis. . . . . ***Page 865***

Imaging and thrombus age: Brighton and colleagues report on the ability of ^{99m}Tc-recombinant tissue plasminogen activator imaging to differentiate recent thrombus formation from older thrombi in patients with deep vein thrombosis. . . . ***Page 873***

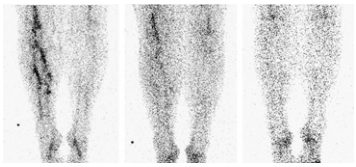

Optimal treatment in pediatric thyroid cancer: Handkiewicz-Junak and colleagues detail the results of a retrospective study investigating combinations of treatments associated with decreased risk of locoregional recurrence in children with differentiated thyroid cancer. . . ***Page 879***

PET and scintigraphy in bone metastases: Ito and colleagues compare the effectiveness of whole-body ^{18}F-FDG PET and ^{99m}Tc bone scintigraphy in detecting metastases in patients with differentiated thyroid cancer after thyroidectomy and before ^{131}I therapy. . . . . ***Page 889***

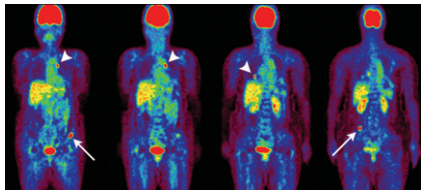

Diffuse thyroid ^{18}F-FDG uptake: Karantanis and colleagues explore the clinical significance of diffusely increased ^{18}F-FDG uptake in the thyroid gland as an incidental finding on PET/CT. . . ***Page 896***

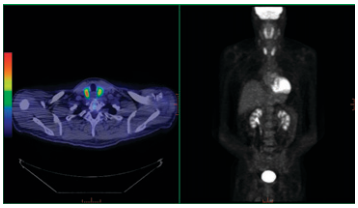

Dual-tracer PET/CT in liver cancer: Ho and colleagues describe the complementary roles of ^{11}C-acetate and ^{18}F-FDG tracers in the PET component of PET/CT detection of metastatic hepatocellular carcinoma. . . . . ***Page 902***

PET/CT registration in liver imaging: Vogel and colleagues evaluate the effect of breathing motion differences on registration accuracy in PET and CT imaging of the liver and offer recommendations on scanner requirements, breath-hold protocols, and reporting. . . . . ***Page 910***

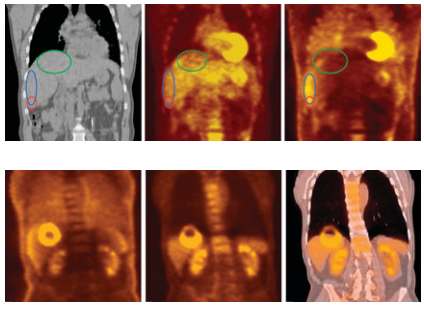

Granulocyte CSF, ^{18}F-FDG, and SUVs: Doot and colleagues determine whether chemotherapy and treatment with granulocyte colony–stimulating factor change blood clearance curves and, therefore, affect the relationship between ^{18}F-FDG metabolic rates and standard uptake values. . .***Page 920***

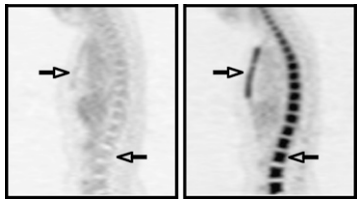

Optimal metabolite curve fitting: Wu and colleagues assess the adequacy of "fit" of 4 metabolite models for correction of arterial input function using data from individuals imaged with ^{11}C-WAY 100635 PET. . . . . ***Page 926***

Partial-volume effect in PET: Soret and colleagues provide an educational overview of the partial-volume effect and its consequences in PET tumor imaging, along with correction models and suggested actions to reduce potential error. . . . . ***Page 932***

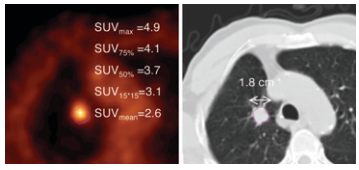

PET imaging of perinatal inflammation: Kannan and colleagues explore small-animal ^{11}C-labeled tracer PET imaging of microglial activation as an indicator of inflammation and perinatal brain injury. . . . ***Page 946***

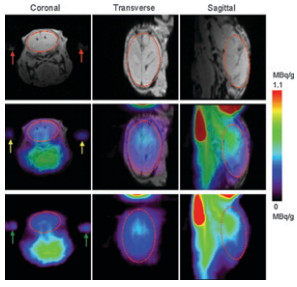

PET and myocardial glucose metabolism: Herrero and colleagues investigate whether compartmental modeling of 1-^{11}C-glucose PET kinetics can be used for noninvasive measurement of myocardial glucose metabolism beyond its initial extraction. . . . . ***Page 955***

Novel tumor-binding peptide: Zitzmann and colleagues describe the binding properties and pharmacokinetic behavior of a new radiolabeled peptide in both in vitro and in vivo models of follicular thyroid carcinoma. . . . ***Page 965***

PET in hypoxia-directed radiochemotherapy: Beck and colleagues report on the ability of small-animal PET using the hypoxia tracer ^{18}F-FAZA to predict the success of radiotherapy in combination with tirapazamine, a specific cytotoxin for hypoxic cells. . . . ***Page 973***

Nicotine and brown adipose tissue uptake: Baba and colleagues evaluate the effects of β-adrenergic agonists on ^{18}F-FDG uptake in brown adipose tissue in rats and offer cautions about the effects of nicotine on PET imaging. . . . . ***Page 981***

PET melanocortin receptor expression imaging: Cheng and colleagues investigate ^{18}F-FB-NAPamide as a promising molecular probe for α-melanocyte-stimulating hormone receptor–positive melanoma and describe initial studies in mice. . . . ***Page 987***

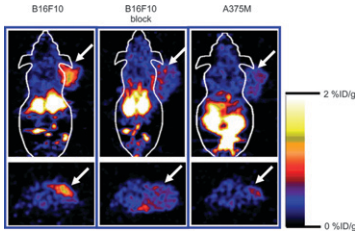

Antibody penetration in tumor tissue: Thurber and colleagues address the complexities of and kinetic barriers to tumor targeting in antibody-based therapeutics with a theoretical model that suggests that such therapies may be better suited to micrometastases than vascularized tumors. . . . . ***Page 995***

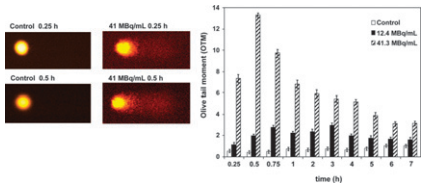

DNA nanoirradiation and cell kill: Reske and colleagues investigate whether selective nanoirradiation of DNA with Auger electrons emitted by ^{123}I-ITdU can induce apoptosis and break resistance to doxorubicin, β-, and γ-irradiation in leukemia cells. . . ***Page 1000***

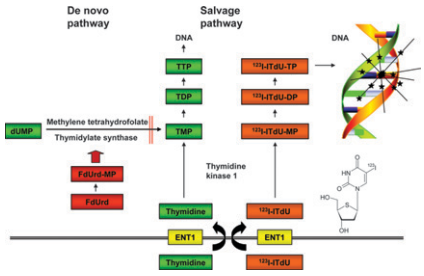

3D radiobiologic dosimetry: Prideaux and colleagues use data from a ^{131}I-treated patient to create radiobiologic modeling that converts the spatial distribution of absorbed dose into biologically effective dose and equivalent uniform dose parameters. . . . . ***Page 1008***

Anti*-^{18}F-FACBC dosimetry:** Nye and colleagues evaluate the human whole-body radiation burden of *anti*-^{18}F-FACBC, a recently developed ligand that permits PET evaluation of the L-amino acid transport system. . . . . ***Page 1017

PET and coronary artery stenosis: Madar and colleagues report on the potential clinical utility of ^{18}F-FBnTP PET in assessing the severity of coronary artery stenosis in a canine model. . . ***Page 1021***

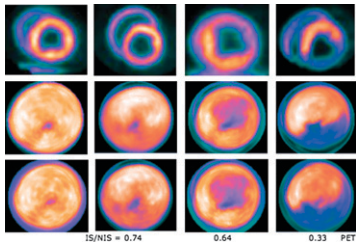

Imaging cardiac cell death: Zhu and colleagues characterize the temporal and spatial distribution of a ^{99m}Tc-labeled fusion protein of C2A and glutathione-s-transferase in a rat model of myocardial ischemia and reperfusion. . . . ***Page 1031***

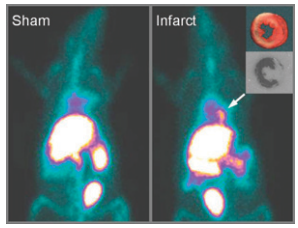

ON THE COVER

^{18}F-FDG PET/CT has been found useful in evaluating hepatocellular carcinoma metastases, although its role in the diagnosis of primary hepatocellular carcinoma is more limited. Dual-tracer PET/CT with ^{18}F-FDG and ^{11}C-acetate has shown an incremental value and a complementary advantage over single-tracer imaging in the evaluation of hepatocellular carcinoma metastases. Some intrathoracic nodes showing increased ^{18}F-FDG activity could be noncalcified granulomatous nodes and, thus, false-positive for metastasis. This possibility can be minimized by correlating serial PET/CT with other ancillary findings.

SEE PAGE 908